ISBN: 978-3-95450-236-3 ISSN: 2673-5350 doi:10.18429/JACoW-IBIC2023-WEP021

100 Hz X-RAY BEAM PROFILE MEASUREMENTS FROM A TRANSMISSIVE CVD DIAMOND DETECTOR

C. Bloomer*[1], L. Bobb, Diamond Light Source, Oxfordshire, UK
M.E. Newton, University of Warwick, Coventry, UK
[1]also at University of Warwick, Coventry, UK

Abstract

A non-destructive CVD diamond X-ray beam imaging monitor has been developed for synchrotron beamlines. The device can be permanently installed in the X-ray beam path and is capable of transmissively imaging the beam profile at 100 frames per second. The response of this transmissive detector at this imaging rate is compared to synchronously acquired images using a destructive fluorescent screen. It is shown that beam position, size, and intensity measurements can be obtained with minimal disturbance to the transmitted X-ray beam. This functionality is beneficial to synchrotron beamlines as it enables them to monitor the X-ray beam focal size and position in real-time, during user experiments. This is a key enabling technology that would enable live beam size feedback, keeping the beamline's focusing optics optimised at all times. Ground vibrations (10 Hz - 20 Hz) can cause movement of focusing optics and beamline mirrors, which disturb the X-ray beam and reduce the ultimate quality of the sample-point beam. This instrument can detect this beam motion, enabling the source to be more easily determined and mitigations to be put in place.

INTRODUCTION

Diamond detectors for synchrotron X-ray beamlines are advantageous for a number of reasons. Firstly, diamond is highly transparent to X-rays compared to other detector materials, which enables it to be installed permanently on the beamline in the beam path. Secondly, diamond has favourable thermal properties such high melting point and heat conduction, that enable it to withstand intense X-ray beams from synchrotrons and XFELs. Thirdly, the strong diamond lattice is both physically robust and resistant to mechanical damage, and it is radiation tolerant. Finally, and of particular use for this form of detector, the diamond structure can be modified by fast laser pulses, to 'write' laser conductive wires and electrodes within the bulk diamond [1]. The results presented in this contribution are from a pixellated single-crystal CVD diamond with laser written electrodes. The design of the 10 x 11 pixel detector and initial results from synchrotrons and XFELs are presented in Refs. [2–5], along with discussion of the advantages and disadvantages of diamond for this application.

To briefly summarise the design and operation of this prototype pixellated diamond detector, it builds upon a concept first presented in Ref. [6]. A pattern of 'strip electrodes' on one face of a diamond plate could be sequentially biased, while the subsequent charge reaching a pattern of orthogonal electrodes on the opposite face of the diamond is read out using electrommeters or other sensitive ammeters. Sequentially biasing the 'strip electrodes' enables one row of pixels to the read out at a time. The graphitic wire detector improves upon this design in two respects: firstly, through the use of laser-written graphitic electrodes which are buried under the surface of the diamond plate, protecting them from damage and resulting in a more physically robust detector; and secondly, through a novel lock-in modulated bias technique, illustrated in Fig. 1, whereby all 'bias' electrodes simultaneously have an AC bias applied to them at different frequencies using a programmable multi-channel DAC. The resulting signal currents from each 'measurement' electrode are simultaneously acquired using a multi-channel 20 kS / s acquisition system. A Fourier transform of the signal currents from each measurement electrode is carried out. The Fourier amplitude of the measured signal at a given frequency is proportional to the flux passing through the detector at the intersection between the measurement electrode and the bias electrode modulated by that frequency.

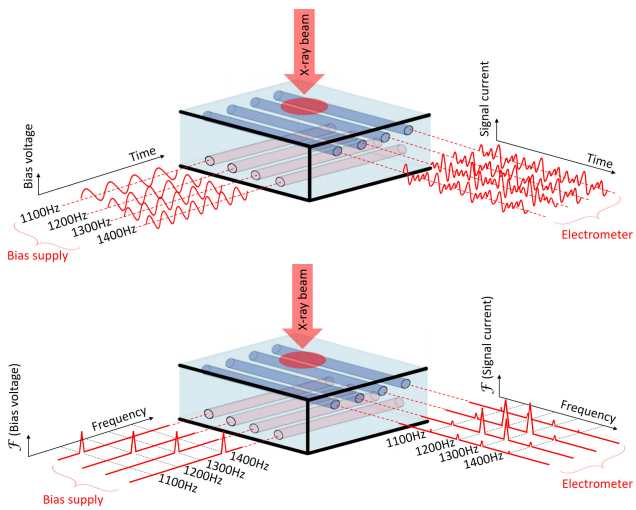

Figure 1: A sketch of the pixel readout scheme, utilising a different modulation frequency applied to each graphitic 'bias' electrode. Top: A time-domain view of the modulation scheme. Bottom: A frequency-domain view, showing how the individual modulation frequencies measured by the electrometer build up a picture of the X-ray beam profile.

* chris.bloomer@diamond.ac.uk

ISBN: 978-3-95450-236-3 ISSN: 2673-5350 doi:10.18429/JACoW-IBIC2023-WEP021

OBTAINING 100 FRAME PER SECOND IMAGES

Experiments were carried out on the I18 beamline at Diamond Light Source [7]. A photon energy of 15 keV was selected, providing a collimated photon beam with a flux of up to 3×10^{11} ph / s. The beam size at the detector could be altered from 20 µm up to 250 µm FWHM through the use of adjustable focusing mirrors.

The diamond graphitic wire detector and a traditional fluorescent screen system (a CMOS camera recording the fluorescence from a cerium-doped lutetium-aluminium-garnet, LuAG:Ce, fluorescent screen) were installed together at the focal point, supported on a motion stage which allowed them to be aligned to the incident beam. The transparent graphitic wire detector (15 keV photon absorption < 5 %) was installed ~ 10 mm upstream of the opaque LuAG:Ce fluorescent screen (15 keV photon absorption > 80 %) [3, 8].

Figure 2 presents the sum of the discrete Fourier transform (DFT) from all of the 11 measurement channels, up to 6 kHz, when it was illuminated by a large, 200 µm FWHM. The modulation frequencies used are highlighted. In this image one can see how the 1-dimensional beam profile is determined from the amplitude of the Fourier transform of the modulation frequencies. The individual signal currents obtained from each of the 11 readout channels from the graphitic wire detector beam are presented in Fig. 3. This figure shows the resulting DFT of these signals from a 1 s (top) and 10 ms acquisition period (bottom).

The acquisition goal of 100 frames per second (FPS) was chosen as this would enable any X-ray beam motion arising from the most common 'ground vibration' frequencies at Diamond Light Source, around 10 Hz - 20 Hz, to be clearly measured.

The bias modulation frequencies used were 1.0 kHz, 1.1 kHz, 1.2 kHz, ..., 1.9 kHz. This choice of modulation frequencies has been carefully chosen:

- Firstly, these frequencies easily allows for short acquisition periods of just 10 ms, enabling 100 FPS acquisition of the images. With a 20 kHz sampling rate, a 10 ms acquisition will contain 200 samples. The DFT of these samples will result in each of the modulation frequencies occupying exactly one frequency bin, simplifying the image acquisition. Each frequency bin of the DFT corresponds to one column of pixels on the detector. The bottom plot in Fig. 3 presents the Fourier transform from one 10 ms acquisition to illustrate this.
- Secondly, it ensures that the lowest modulation frequency used, 1.0 kHz is well above the frequency of any *beating* between neighbouring modulation frequencies, observed at 100 Hz, 200 Hz, 300 Hz, etc.
- Lastly, it ensures that higher harmonics of the chosen modulation frequencies will not clash with any of the modulation frequencies themselves: the lowest modulation frequency, 1.0 kHz, has a 2nd harmonic that is above the highest modulation frequency of 1.9 kHz.

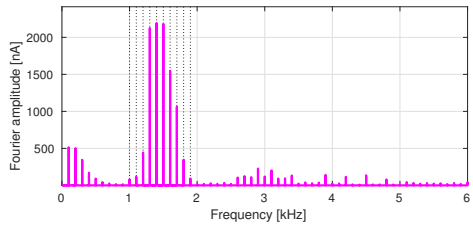

Figure 2: The sum of the individual DFT results from the 11 measurement channels, showing obtained spectra from 1 Hz to 6 kHz calculated from 1 second of data acquired at 20 kHz. These results show the appearance of lower frequency 'beating' and higher frequency harmonics of the main modulation frequencies.

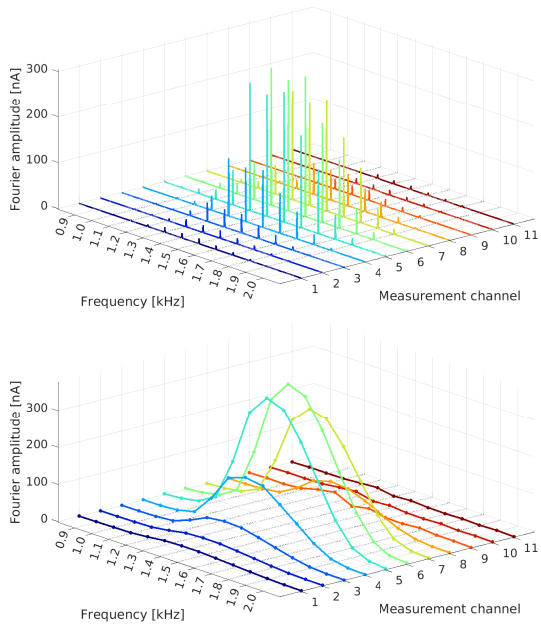

Figure 3: The Fourier transforms from 20 kHz signals acquired from 11 measurement electrodes whilst the X-ray beam is illuminating the detector. These plots just show the DFT amplitudes from 0.9 kHz to 2.0 kHz, around the modulation frequencies used. Top: The Fourier transform of a 1 second long acquisition at 20 kHz signals. Bottom: The Fourier transform of a 10 ms acquisition.

ESTIMATED POINT SPREAD FUNCTION AND IMAGE DECONVOLUTION

By illuminating the detector with as small an X-ray beam as possible an estimate of the 2-dimensional point spread function (PSF) of the detector can be measured. To make this estimate, the beamline optics were used to focus the X-ray beam down to the smallest beamsize achievable at the location of the detector. The resulting beamsize at the detector was measured to be 24 µm x 20 µm FWHM, as measured by two independent means: firstly by direct X-ray camera image, and secondly by knife-edge measurement. This is much smaller than one 50 µm x 50 µm pixel of the graphitic wire detector and is sufficient to make a reasonable estimate of

ISBN: 978-3-95450-236-3 ISSN: 2673-5350 doi:10.18429/JACoW-IBIC2023-WEP021

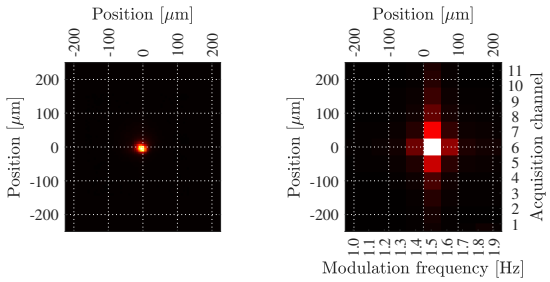

Figure 4: Acquired images of the 24 µm x 20 µm FWHM X-ray beam. Left: The fluorescent screen image of the incident beam profile. Right: The measured estimate of the PSF of the graphitic wire detector, obtained by illuminating the detector with the small incident beam size. Both images depict the same field of view.

the PSF. Under this illumination the obtained 2-dimensional image obtained using both the fluorescent screen monitor and the graphitic wire detector is presented in Fig. 4.

It is clear that there is some 'spread' of the signal across multiple pixels of the graphitic wire detector. Of particular note is that this obtained PSF does not exhibit the radial symmetry that one would anticipate from an ideal detector. There is a vertical spread of the measured beam profile, smearing the 20 µm vertical beam profile across several 50 µm sized pixels. Horizontally there is only a small amount of spread, into only the neighbouring pixels. This asymmetrical response in the vertical and horizontal directions is not entirely unexpected, as the acquisition methods differ in the two axes: each pixel in a horizontal 'row' is defined by a different modulation frequency; each pixel in a vertical vertical column is obtained from a separate measurement channel (as indicated by the axes in Fig. 4). It becomes clear that the frequency of the centre electrode being struck by the incident beam, 1500 Hz in this case, is 'leaking' across the various measurement channels.

As we have obtained a good estimate of the PSF, and confirmed that the PSF is consistent across the face of the graphitic wire detector, image deconvolution algorithms can be introduced to estimate the original beam profile from the detector image. A commonly used method originating from the fields of optics and astronomy is the Richardson-Lucy algorithm [9, 10]. The deconvolution was carried out using MathWorks MATLAB, with the built-in `deconvlucy` function [11]. The default algorithm tuning parameters of the function were used. The results of these reconstructions are presented in Fig. 5.

IMAGING RESULTS

To demonstrate the 100 frame per second (FPS) capabilities of the detector, the motion stage was used to oscillate both the graphitic wire detector and the fluorescent screen back and forth relative to the incident beam. For both detectors, a 2-dimensional Gaussian fit was used to find the beam centroid. The CMOS camera observing the fluorescent screen was configured to acquire data at 100 FPS in free-run mode using an integration period of 1 ms, while the graphitic wire detector signal currents were acquired continuously at 20 kHz and then divided up into 10 ms (100 FPS) chunks for analysis. Acquisition from the two devices was initiated by external hardware trigger. Figure 6 shows the an example of the graphitic wire detector image obtained (after deconvolution using the Richardson-Lucy algorithm) alongside the simultaneously acquired fluorescent screen image, both acquired as part of a 100 FPS sequence. The combined computation time for both the deconvolution and the 2-dimensional Gaussian fit of the graphitic wire detector image using MATLAB was < 4 ms, enabling both to be

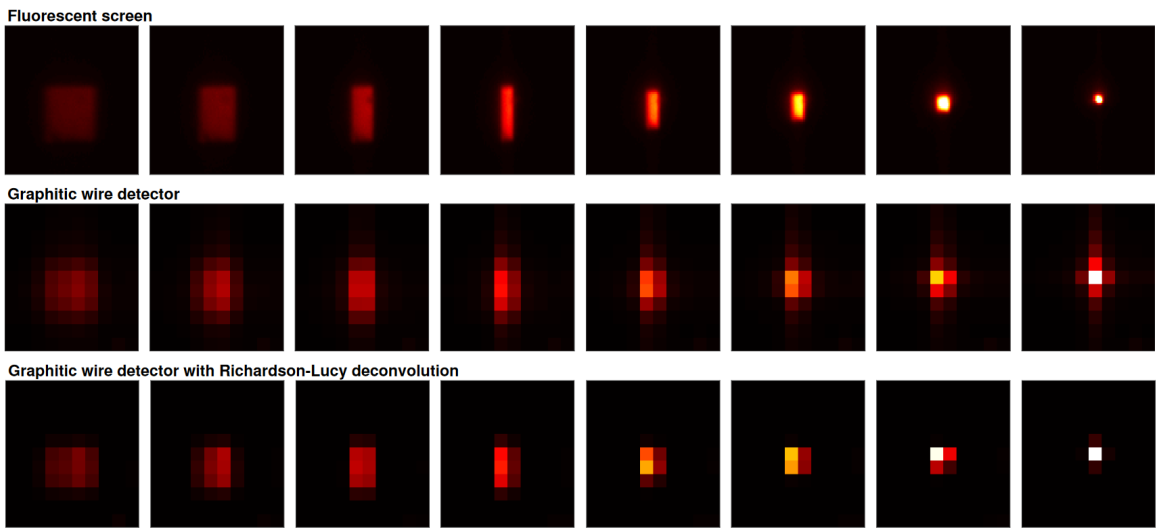

Figure 5: Images obtained of the X-ray beam profile with 10 ms acquisition period during during a beam focusing procedure. Top row: Images obtained from the fluorescent screen. Middle row: Raw images obtained from the graphitic wire detector. Bottom row: The estimated reconstruction of the beam profile obtained using the Richardson-Lucy algorithm.

ISBN: 978-3-95450-236-3 ISSN: 2673-5350 doi:10.18429/JACoW-IBIC2023-WEP021

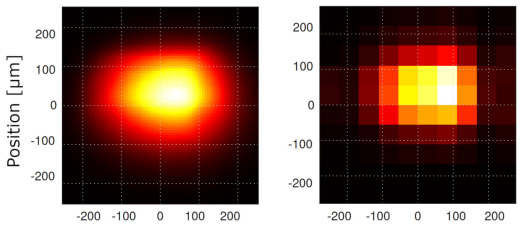

Figure 6: Beam profile images simultaneously acquired using both the the fluorescent screen and CMOS camera (left) and the graphitic wire detector (right). The X, Y measurements shown are units of microns.

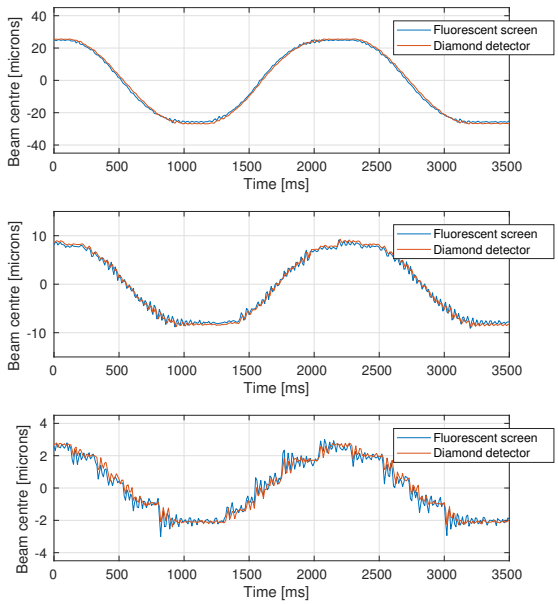

Figure 7: Vertical beam position measurements acquired from 100 FPS image sequences during stepper motor movements of the stage the detector was mounted upon. The motor is requested to move in a sine wave with an amplitude of ± 30 µm (top); ± 10 µm (middle); and ± 3 µm (bottom).

completed in real-time while the following image is being acquired.

Figure 7 shows the measured variation in beam position simultaneously obtained from the 100 FPS images from both the graphitic wire detector and from the fluorescent screen image for a series of 1-dimensional vertical stepper motor sweeps. The first sweep (top) is a ± 30 µm sine wave requested from the motor; the second (middle) is a ± 10 µm motor request; the final motion (bottom) shows the results when a ± 3 µm sine wave was requested. This final sweep was at the limit of the motor's capability, and it is clear from the obtained position measurements that the motor cannot reproduce a smooth sine wave, instead a series of discrete steps is observed, with some settling time and 'rattling' after each step. Both the graphitic wire detector and the fluorescent screen images observe the same effect. The use of 2-dimensional Gaussian fitting enables these motions to be observed on the graphitic wire detector even though they are clearly significantly smaller than the 50 µm pixel size.

CONCLUSIONS

The graphitic wire detector presented in this work is shown to successfully obtain X-ray beam images and beam position measurements. A novel lock-in modulation readout method has been demonstrated, enabling 100 FPS acquisition of 2-dimension X-ray beam profile and centroid measurements. All pixels were acquired simultaneously.

The position measurement results are comparable to that obtained from a traditional fluorescent screen, however the X-ray absorption is significantly less than most fluorescent materials. The graphitic wire detector may be permanently installed in the X-ray beam path, offering significant advantages over fluorescent screens or knife-edge scans which generally cannot be used during user experiments as they intercept too great a portion of the synchrotron flux or block it entirely.

While the PSF of the detector shows 'leakage' into neighbouring pixels and does not exhibit radial symmetry, a software deconvolution approach has been demonstrated to reconstruct the beam profile satisfactorily, and enable submicron beam position measurement.

Possible future developments include both smaller pixel sizes, as the laser writing steps could easily be changed to implement a pixel pitch down to ~ 15 µm, and higher pixel counts, as this experiment was limited by the number of available ADC channels. Using higher sample rate DACs and ADCs would also enable an increase in the frame rate, if required. There are commercially available 32-channel DAC and ADC units capable of 100 kHz output/input which could be used to increase both the pixel count and the acquisition rate.

This detector is beneficial to synchrotron beamlines as it enables scientists and users to monitor the X-ray beam focal size and position in real-time, during user experiments. This functionality would enable live feedback, keeping the beamline focusing optics optimised at all times. It would reduce set-up and commissioning time, as the detector can be permanently installed in the X-ray beam path and beam sizes can be determined without having to temporarily insert destructive monitors into the beam path.

ACKNOWLEDGEMENTS

The authors wish to acknowledge the support of many individuals and groups that aided in this research. The CVD diamond plate used was provided by Element Six. We wish to acknowledge the contributions of P. Salter for the graphitic electrode fabrication, at the University of Oxford. The detector surface metallisation was carried out by B. Green, and the wire bonding by F. Courtney, both at the University of Warwick. We are grateful for the support of G. Cook and K. Ignatyev at Diamond Light Source for their help in carrying out these experiments.

REFERENCES

[1] B. Sun *et al.*, "High conductivity micro-wires in diamond following arbitrary paths", *Appl. Phys. Lett.* , vol. 105, p. 231105,

ISBN: 978-3-95450-236-3 ISSN: 2673-5350 doi:10.18429/JACoW-IBIC2023-WEP021

2014. doi:10.1063/1.4902998

[2] C. Bloomer *et al.*, "A single-crystal diamond X-ray pixel detector with embedded graphitic electrodes", *J. Synchrotron Radiat.*, vol. 27, pp. 599–607, 2016. doi:10.1107/s160057752000140x

[3] C. Bloomer, L. Bobb, and M. E. Newton, "Single-Crystal Diamond Pixelated Radiation Detector with Buried Graphitic Electrodes", in *Proc. IBIC'21*, Pohang, Korea, Sep. 2021, pp. 158–166. doi:10.18429/JACoW-IBIC2021-TUOA01

[4] C. Bloomer *et al.*, "XFEL Photon Pulse Measurement Using an All-Carbon Diamond Detector", in *Proc. IBIC'22*, Kraków, Poland, Sep. 2022, pp. 416–420. doi:10.18429/JACoW-IBIC2022-WEP15

[5] C. Bloomer, "A Pixelated CVD Diamond Synchrotron Radiation Monitor with Graphitic Electrodes", Ph.D. Thesis, Dept. of Phys., University of Warwick, UK, 2023.

[6] D. Shu *et al.*, "CVD-diamond-based position sensitive photoconductive detector for high-flux X-rays and gamma rays", *Proceedings of the Particle Accelerator Conference*, pp. 2090-2092, 1999. https://jacow.org/p99/PAPERS/WEA90.PDF

[7] J. Mosselmans *et al.*, "I18 - the microfocus spectroscopy beamline at the Diamond Light Source", *J. Synchrotron Radiat.*, vol. 16, pp. 818–824, 2009. doi:10.1107/S0909049509032282

[8] B. L. Henke *et al.*, "X-ray interactions: photoabsorption, scattering, transmission, and reflection at E=50-30000 eV, Z=1-92", *At. Data Nucl. Data Tables*, vol. 54, pp. 181–342, 1993. doi:10.1006/adnd.1993.1013

[9] W.H. Richardson, "Bayesian-based iterative method of image restoration", *J. Opt. Soc. Am.*, vol. 62, 1972. doi:10.1364/josa.62.000055

[10] L.B. Lucy, "An iterative technique for the rectification of observed distributions", *Astron. J.*, vol. 79, 1974. doi:10.1086/111605

[11] Mathworks, "Deblurring Images Using the Lucy-Richardson Algorithm", 2021. https://uk.mathworks.com/help/images/deblurring-images-using-the-lucy-richardson-algorithm.html